Absolute cross section for positron-impact ionization of hydrogen near threshold

Krista Jansen,[1] S. J. Ward,[1] J. Shertzer,[2] and J. H. Macek[3]
[1]*Department of Physics, University of North Texas, Denton, Texas 76203, USA*
[2]*Department of Physics, College of the Holy Cross, Worcester, Massachusetts 01610, USA*
[3]*Department of Physics and Astronomy, University of Tennessee, Knoxville, Tennessee 37996, USA and Oak Ridge National Laboratory, Oak Ridge, Tennessee 37831, USA*
(Received 3 October 2008; published 5 February 2009)

We investigate positron-impact ionization of hydrogen near threshold using the hyperspherical hidden crossing method (HHCM). Previously, Ihra *et al.* [Phys. Rev. Lett. **78**, 4027 (1997)] used the HHCM to obtain the extended Wannier threshold law for zero angular momentum. We extend their analysis to higher angular momentum L and show that the extended Wannier threshold law is L independent. We also calculate the absolute partial-wave ionization cross sections for $L=0$, 1, 2, and 3 and compare our results with other calculations and with experimental measurements. The HHCM calculation provides an explanation for the very small S-wave and large D-wave contributions to the ionization cross section in terms of destructive and constructive interference, respectively.

DOI: 10.1103/PhysRevA.79.022704 PACS number(s): 34.10.+x, 34.80.Uv

I. INTRODUCTION

The behavior of the cross section for positron-hydrogen ionization near threshold is a very sensitive test of three-particle correlations. Positron collisions differ from electron collisions in two distinctive ways: exchange due to the Pauli exclusion principle is absent, but positronium formation is possible.

Using a classical treatment, Wannier obtained for electron-impact ionization of neutral atoms the energy dependence of the cross section $\sigma(E)$ near threshold:

$$\sigma(E) \propto E^{\zeta}, \tag{1}$$

where E is the excess energy and the exponent is $\zeta=1.127$ [1]. In the Wannier configuration for electron-impact ionization of hydrogen, the proton and two electrons are collinear, with the proton exactly at the midpoint between the two electrons.

Klar [2] showed that for positron-impact ionization of neutral atoms the exponent is $\zeta=2.650\,11$. In the Wannier configuration for positron-hydrogen ionization, the three charged particles lie along a line with the electron approximately midway between the positron and the proton.

Positron-hydrogen ionization is of both experimental and theoretical interest. The cross section for this process has been measured for kinetic energies in the range 15–700 eV [3]. There have been relatively few calculations of positron-hydrogen ionization that focus on the near-threshold energy region. Rost and Heller [4] performed a semiclassical calculation to compute the S matrix near the ionization threshold for angular momentum $L=0$. By considering the phase-space variables of the classical Hamiltonian, they made the important conclusion that the energy dependence of the cross section near threshold is independent of L.

Using the hyperspherical hidden crossing method (HHCM) [5] Ihra *et al.* [6] derived quantum mechanically the Wannier threshold law for $L=0$ for positron-hydrogen ionization. They also calculated a correction term for $L=0$ which extends the Wannier threshold law to higher energies. They expanded the three-particle potential around the Wannier saddle point by taking into account the anharmonic terms perturbatively. The extended Wannier threshold law was used to explain measurements of positron-helium ionization near threshold [7]. However, the calculation was for the S wave only, and the cross section computed was relative. It should be noted that Deb and Crothers [8] performed a quantal semiclassical calculation for positron impact ionization of helium near threshold that agreed with the experimental measurements [7]. In their paper, they stressed the importance of the higher partial waves.

There have been a number of close coupling (CC) calculations of positron-hydrogen ionization over a wide energy range [9–11]. An elaborate CC calculation was performed by Kernoghan *et al.* [11] who used a 33-state basis to compute the total ionization cross section for positron impact energies up to 110 eV. However, the 33-state CC calculation of the total ionization cross section does not satisfy the Wannier threshold law.

Recently, Kadyrov and co-workers [12–14] applied the convergent close coupling (CCC) method to positron-hydrogen ionization. They performed a detailed calculation for the S wave near threshold by using two different S-wave models. In one S-wave model, only the s states of hydrogen and positronium are retained [13]; in the other model, the s, p, and d states are retained [14]. The S-wave ionization cross section obtained using the S-wave model where the s states of hydrogen and positronium are retained is in accord with the Wannier threshold law. For the S-wave model in which the s, p, and d states are retained, the calculation could not be extended below 1 eV due to computational difficulties. Kadyrov and co-workers [12,13] also performed a full CCC calculation for the total ionization cross section. However, for the full CCC calculation, the numerical equations become highly ill conditioned in the near-threshold region.

In this paper, we extend the HHCM calculation of near-threshold positron-hydrogen ionization [6,15] to higher partial waves. We prove that the extended Wannier threshold law has the same form for all L. We also determine the absolute ionization cross sections for $L=0$, 1, 2, and 3. Re-

cently, we reported a preliminary calculation of the ionization cross section for $L=0$, 1, and 2 [16] in which we used the 18-state CC cross section of ground-state positronium formation [10]. Here, we compute the ionization cross section entirely within the framework of the HHCM and include the important $L=3$ contribution.

The HHCM was formulated specifically to treat the correlated motion of three charged particles [5]. The method has a number of important features that makes it ideally suited for treating positron-hydrogen ionization near threshold. A very important feature of the HHCM is that it can be applied at energies extremely close to threshold. The cross section for electron-impact ionization of hydrogen near threshold computed with the HHCM is in accord with the Wannier threshold law [5,17]. An important feature of hyperspherical-based methods is that these methods do not suffer from overcompleteness of the basis [18]; this can be a problem in CC calculations where an expansion is made about both the target and positronium states. The HHCM provides valuable insight into scattering processes. For instance, the method has provided an interpretation for the very small S-wave and significant D-wave cross sections for positronium formation in positron-hydrogen collisions in the Ore gap [19], and for the very small S-wave positronium formation cross section for low-energy positron-lithium collisions [20,21].

In Sec. II, we apply the HHCM to positron-impact ionization of hydrogen near threshold for arbitrary L. In Sec. III, we present the HHCM results and compare them to other calculations [11–14] and experimental data [3]. In Sec. IV, we give the conclusions. We use atomic units throughout the paper except when explicitly stated otherwise.

II. APPLICATION OF THE HHCM TO NEAR-THRESHOLD POSITRON-HYDROGEN IONIZATION

A. Expansion of the eigenvalue $2\varepsilon'(R)R^2$

The HHCM for three charged particles was formulated [5] using hyperspherical coordinates R and $\hat{\mathbf{R}}$, where the hyperradius R is the sum of the squares of mass-scaled center-of-mass coordinates of the three particles and the remaining coordinates $\hat{\mathbf{R}}$ are a set of hyperangles [18,22]. For positron-hydrogen collisions, it is appropriate to use the hyperspherical coordinates given by the hyperradius $R=\sqrt{r_+^2+r_-^2}$ and Ω, where Ω denotes the hyperangle $\alpha=\tan^{-1}(r_-/r_+)$, $\theta=\cos^{-1}(\hat{\mathbf{r}}_+\cdot\hat{\mathbf{r}}_-)$, and the three Euler angles $(\omega_1,\omega_2,\omega_3)$ which specify the orientation of the body-fixed frame [23]. $\mathbf{r}_+$ and $\mathbf{r}_-$ are the position vectors of the positron and electron, respectively, relative to the proton, which we take to be infinitely massive [23]. Defining the reduced wave function $\Psi(R,\Omega)$ in terms of the standard wave function $\psi(R,\Omega)$,

$$\Psi(R,\Omega)=R^{5/2}\sin\alpha\cos\alpha\psi(R,\Omega), \tag{2}$$

the Schrödinger equation can be written as

$$\left[-\frac{\partial^2}{\partial R^2}+\frac{\Lambda^2+2RC(\alpha,\theta)}{R^2}-2E\right]\Psi(R,\Omega)=0, \tag{3}$$

where Λ^2 is the grand angular momentum operator [23]. We show the reduced potential, which is given by

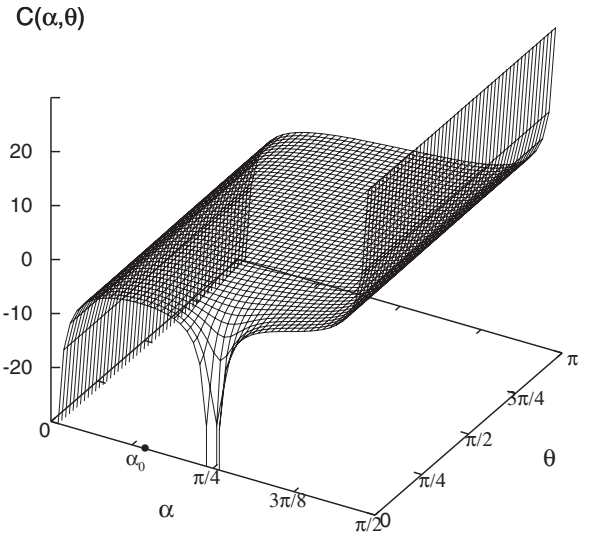

FIG. 1. The reduced potential $C(\alpha,\theta)$. The saddle point is at $(\alpha_0,\theta_0)=(0.4347,0)$.

$$C(\alpha,\theta)=\frac{1}{\cos\alpha}-\frac{1}{\sin\alpha}-\frac{1}{(1-\sin 2\alpha\cos\theta)^{1/2}}, \tag{4}$$

in Fig. 1. E is the total energy of the system, which for positron-hydrogen ionization is the same as the excess energy. The adiabatic basis functions $\varphi_\mu(R;\Omega)$ are the eigenstates of the adiabatic Hamiltonian where R is held fixed:

$$[\Lambda^2+2RC(\alpha,\theta)]\varphi_\mu(R;\Omega)=2R^2\varepsilon_\mu(R)\varphi_\mu(R;\Omega). \tag{5}$$

We expand the adiabatic function $\varphi_\mu(R;\Omega)$ into states of total angular momentum L [17,23],

$$\varphi_\mu(R;\Omega)=\sum_{I=0}^{L}f_{I,\mu}^L(R;\alpha,\theta)\tilde{\mathcal{D}}_{I,M}^L(\omega_1,\omega_2,\omega_3), \tag{6}$$

where I is the projection of the total angular momentum onto the body-fixed z' axis, M is the projection onto the spaced-fixed z axis, and $\tilde{\mathcal{D}}_{I,M}^L(\omega_1,\omega_2,\omega_3)$ are the normalized and symmetrized vector spherical harmonics [23,24]. Substituting Eq. (6) into Eq. (5) we obtain a set of $L+1$ coupled partial differential equations,

$$\sum_{I'=0}^{L}H_{II'}f_{I'}(R;\alpha,\theta)=2R^2\varepsilon'(R)f_I(R;\alpha,\theta),\quad I=0,1,2\ldots L, \tag{7}$$

where $2R^2\varepsilon'(R)=2R^2\varepsilon(R)+\frac{1}{4}$. For brevity of notation, we suppress the μ index on $f_I(R;\alpha,\theta)$, $\varepsilon'(R)$ and $\varepsilon(R)$; we also suppress the L index on $H_{II'}$, $f_I(R;\alpha,\theta)$, $\varepsilon'(R)$, and $\varepsilon(R)$. The operators $H_{II'}$ (in Rydberg units) associated with the tridiagonal matrix $\mathbf{H}$ are

$$H_{II}=-\frac{\partial^2}{\partial\alpha^2}-\frac{1}{\sin^2\alpha\cos^2\alpha}\left(\frac{\partial^2}{\partial\theta^2}+\cot\theta\frac{\partial}{\partial\theta}-\frac{I^2}{\sin^2\theta}\right)+\frac{L(L+1)-2I^2}{\cos^2\alpha}+2RC(\alpha,\theta),$$

$$H_{I,I+1} = -\frac{\sqrt{(L+I+1)(L-I)(1+\delta_{I,0})}}{\cos^2\alpha}\left(\frac{\partial}{\partial\theta} + (I+1)\cot\theta\right),$$

$$H_{I,I-1} = \frac{\sqrt{(L-I+1)(L+I)(1+\delta_{I,1})}}{\cos^2\alpha}\left(\frac{\partial}{\partial\theta} - (I-1)\cot\theta\right). \tag{8}$$

Our interest here is in near-threshold ionization, where the wave function is localized in the region of space near the saddle point as $R\to\infty$. The saddle point in the reduced potential $C(\alpha,\theta)$ (see Fig. 1) is located at $(\alpha_0,\theta_0)=(0.4347,0)$, corresponding to the collinear configuration of the proton, electron, and positron in which the ratio of the lengths is $r_-/r_+=0.4643$.

We define coordinates $x=\alpha-\alpha_0$ and $y=\theta-\theta_0$ and carry out a Taylor series expansion of the matrix $\mathbf{H}$ about the point $(x,y)=(0,0)$. We group the terms as $\mathbf{H}=-2RC_{00}\mathbf{1}+\mathbf{H}^0+\mathbf{H}^1+\mathbf{H}^2$ where

$$H^0_{II} = -\frac{\partial^2}{\partial x^2} - B_0\left(\frac{\partial^2}{\partial y^2} + \frac{1}{y}\frac{\partial}{\partial y} - \frac{I^2}{y^2}\right) + 2R(-C_{20}x^2 + C_{02}y^2),$$

$$H^1_{II} = B_1 x\left(\frac{\partial^2}{\partial y^2} + \frac{1}{y}\frac{\partial}{\partial y} - \frac{I^2}{y^2}\right) + 2R(-C_{30}x^3 + C_{12}xy^2),$$

$$H^2_{II} = B_0\left(\frac{y}{3}\frac{\partial}{\partial y} + \frac{I^2}{3}\right) - B_2x^2\left(\frac{\partial^2}{\partial y^2} + \frac{1}{y}\frac{\partial}{\partial y} - \frac{I^2}{y^2}\right) + 2R(C_{22}x^2y^2 - C_{40}x^4 - C_{04}y^4) + D_0[L(L+1) - 2I^2],$$

$$H^0_{I,I+1} = 0,$$

$$H^1_{I,I+1} = -\sqrt{(L+I+1)(L-I)(1+\delta_{I,0})}D_0\left(\frac{\partial}{\partial y} + \frac{(I+1)}{y}\right),$$

$$H^2_{I,I+1} = -\sqrt{(L+I+1)(L-I)(1+\delta_{I,0})}D_1x\left(\frac{\partial}{\partial y} + \frac{(I+1)}{y}\right),$$

$$H^0_{I,I-1} = 0,$$

$$H^1_{I,I-1} = \sqrt{(L-I+1)(L+I)(1+\delta_{I,1})}D_0\left(\frac{\partial}{\partial y} - \frac{(I-1)}{y}\right),$$

$$H^2_{I,I-1} = \sqrt{(L-I+1)(L+I)(1+\delta_{I,1})}D_1x\left(\frac{\partial}{\partial y} - \frac{(I-1)}{y}\right). \tag{9}$$

$\mathbf{H}^0$ is the zeroth-order Hamiltonian whose eigenvalue is proportional to $R^{1/2}$. We treat higher-order terms in the expansion of the Hamiltonian with perturbation theory. The matrix elements of $\mathbf{H}^1$ and $\mathbf{H}^2$ that we construct using the zeroth-order eigenfunctions are proportional to $R^{1/4}$ and R^0, respectively. B_j, C_{jk}, and D_j, are the absolute values of the coefficients which arise from the Taylor expansion of $\sin^{-2}\alpha\cos^{-2}\alpha$, $C(\alpha,\theta)$, and $\cos^{-2}\alpha$, respectively; we give these in Table I.

TABLE I. Absolute value of expansion coefficients, B_j, C_{jk}, and D_j.

$B_0=6.85410$	$C_{00}=3.33010$	$C_{12}=16.4677$	$D_0=1.21559$
$B_1=23.1588$	$C_{20}=27.8208$	$C_{40}=197.162$	$D_1=1.12882$
$B_2=86.1023$	$C_{02}=1.66510$	$C_{22}=96.8868$	
	$C_{30}=18.2063$	$C_{04}=2.15939$	

The zeroth-order Hamiltonian $\mathbf{H}^0$ is equivalent to a one-dimensional antiharmonic oscillator in x and a two-dimensional harmonic oscillator in y. The eigenvalues of $(-2RC_{00}\mathbf{1}+\mathbf{H}^0)$ are

$$2R^2\varepsilon'^{(0)}_{n_xn_yI}(R) = -2C_{00}R + 2[-i(n_x+1/2)\tilde{\omega}_x + 2(2n_y+I+1)B_0\tilde{\omega}_y]R^{1/2}, \tag{10}$$

and the corresponding components of the zeroth-order normalized eigenfunctions are

$$f^{(0)}_{n_xn_yI'}(R;x,y) = \delta_{I,I'}N_{n_x}N_{n_yI}H_{n_x}(\omega_x^{1/2}x)e^{-\omega_x x^2/2} \times \omega_y^{I/2}y^I L^I_{n_y}(\omega_y y^2)e^{-\omega_y y^2/2}, \tag{11}$$

where $\omega_x=-i(2C_{20}R)^{1/2}=-i\tilde{\omega}_xR^{1/2}$, $\omega_y=(2C_{02}R/B_0)^{1/2}=\tilde{\omega}_yR^{1/2}$, and n_x and n_y are the harmonic oscillator quantum numbers. (We use the definition of the associated Laguerre polynomials as given in Ref. [25].) The sign of ω_x is chosen so that the eigenfunctions obey the boundary condition for an outgoing wave. H_{n_x} and $L^I_{n_y}$ are the Hermite and associated Laguerre polynomials. To determine the normalization constants, N_{n_x} and N_{n_yI}, we normalize the integral below to unity,

$$\int_{-\infty}^{\infty}dx\int_0^{\infty}ydy[f^{(0)}_{n_xn_yI}(R;x,y)]^2 = 1. \tag{12}$$

This gives $N_{n_x}=(\omega_x/\pi)^{1/4}(2^{n_x}n_x!)^{-1/2}$ and $N_{n_yI}=(2\omega_y n_y!)^{1/2}[(n_y+I)!]^{-1/2}$. We do not take the complex conjugate of $f^{(0)}_{n_xn_yI}(R;x,y)$ in the integral in order to analytically continue the inner product off the real axis. In evaluating the matrix elements for the expansion of $2R^2\varepsilon'(R)$, we also do not take the complex conjugate of $f^{(0)}_{n_xn_yI}(R;x,y)$.

Along the Wannier Ridge as $R\to\infty$, we are interested in the lowest eigenvalue, which to order $R^{1/2}$, is given by

$$2R^2\varepsilon'_{\rm asy}(R) \equiv 2R^2\varepsilon'^{(0)}_{000}(R) = aR + bR^{1/2}, \tag{13}$$

where $a=-2C_{00}$ and $b=-i\tilde{\omega}_x+2B_0\tilde{\omega}_y$. The corresponding asymptotic eigenfunction is

$$\varphi_{\rm asy}(R;\Omega) \equiv f^{(0)}_{000}(R;x,y)\tilde{\mathcal{D}}^L_{0,M}(\omega_1,\omega_2,\omega_3) = N_{n_x=0}N_{n_y=0,I=0}\exp(-\omega_x x^2/2) \times\exp(-\omega_y y^2/2)\tilde{\mathcal{D}}^L_{0,M}(\omega_1,\omega_2,\omega_3). \tag{14}$$

Retaining only the terms in the expansion of $2R^2\varepsilon'(R)$ up to order $R^{1/2}$, one can extract the Wannier threshold law; this law is independent of angular momentum L. In order to de-

rive the extended Wannier threshold law for arbitrary L, we calculate corrections of order R^0 to the asymptotic eigenvalue using perturbation theory.

In first-order perturbation theory, we diagonalize $\mathbf{H}=[-2RC_{00}\mathbf{1}+\mathbf{H}^0+\mathbf{H}^1+\mathbf{H}^2]$ in the basis of the zeroth-order eigenfunctions $f_{00I}^{(0)}$ to find the lowest-order correction to the eigenvalue $2R^2\varepsilon'^{(0)}_{000}(R)$. We expand the lowest unknown eigenvalue λ in powers of R

$$\lambda = aR + bR^{1/2} + \gamma + \cdots, \tag{15}$$

and solve for γ by requiring

$$\begin{vmatrix} \langle \tilde{H}^2_{00}\rangle - \gamma & \langle \tilde{H}^1_{01}\rangle R^{1/4} & 0 & \cdots & 0 \\ \langle \tilde{H}^1_{10}\rangle R^{1/4} & 2B_0\tilde{\omega}_y R^{1/2} + \langle \tilde{H}^2_{11}\rangle - \gamma & \langle \tilde{H}^1_{12}\rangle R^{1/4} & \cdots & 0 \\ 0 & \langle \tilde{H}^1_{21}\rangle R^{1/4} & 4B_0\tilde{\omega}_y R^{1/2} + \langle \tilde{H}^2_{22}\rangle - \gamma & \cdots & 0 \\ \vdots & \vdots & \vdots & \ddots & \vdots \\ 0 & 0 & 0 & \cdots & 2LB_0\tilde{\omega}_y R^{1/2} + \langle \tilde{H}^2_{LL}\rangle - \gamma \end{vmatrix} = 0, \tag{16}$$

where $\langle \tilde{H}^1_{I,I\pm1}\rangle = \langle H^1_{I,I\pm1}\rangle R^{-1/4} = \langle f^{(0)}_{00I}|H^1_{I,I\pm1}|f^{(0)}_{00I\pm1}\rangle R^{-1/4}$ and $\langle \tilde{H}^2_{II}\rangle = \langle H^2_{II}\rangle = \langle f^{(0)}_{00I}|H^2_{II}|f^{(0)}_{00I}\rangle$ are independent of R. This yields a polynomial equation in powers of $R^{1/2}$; the leading order term is

$$(2B_0\tilde{\omega}_y)^{L-1}R^{L/2}L!(2B_0\tilde{\omega}_y\langle \tilde{H}^2_{00}\rangle - 2B_0\tilde{\omega}_y\gamma - \langle \tilde{H}^1_{01}\rangle\langle \tilde{H}^1_{10}\rangle), \tag{17}$$

where

$$\langle \tilde{H}^2_{00}\rangle = -\frac{B_0}{3} + \frac{3C_{40}}{2\tilde{\omega}_x^2} - \frac{4C_{04}}{\tilde{\omega}_y^2} + \frac{iB_2\tilde{\omega}_y}{2\tilde{\omega}_x} + \frac{iC_{22}}{\tilde{\omega}_x\tilde{\omega}_y} + D_0L(L+1), \tag{18}$$

and

$$\langle \tilde{H}^1_{10}\rangle = \langle \tilde{H}^1_{01}\rangle = D_0\sqrt{2L(L+1)\tilde{\omega}_y}. \tag{19}$$

Requiring that the coefficient of the leading order term vanish, we obtain

$$\gamma = -\frac{B_0}{3} + \frac{3C_{40}}{2\tilde{\omega}_x^2} - \frac{4C_{04}}{\tilde{\omega}_y^2} + \frac{iB_2\tilde{\omega}_y}{2\tilde{\omega}_x} + \frac{iC_{22}}{\tilde{\omega}_x\tilde{\omega}_y} + L(L+1). \tag{20}$$

There are additional corrections to $2R^2\varepsilon'_{\mathrm{asy}}(R)$ of the order of R^0 that arise in second-order perturbation theory from $\mathbf{H}^1$. These are given by

$$\begin{aligned}\gamma' &= \sum_{\substack{n_x,n_y=0 \\ n_x=n_y\neq 0}}^{\infty} \frac{\langle f^{(0)}_{000}|H^1_{00}|f^{(0)}_{n_xn_y0}\rangle^2}{(2n_x\tilde{\omega}_x - 4n_yB_0\tilde{\omega}_y)R^{1/2}} \\ &= -\frac{11C_{30}^2}{4\tilde{\omega}_x^4} + \left[\frac{B_1^2\tilde{\omega}_y^2}{2\tilde{\omega}_x^2} + \frac{2C_{12}^2}{\tilde{\omega}_x^2\tilde{\omega}_y^2}\right]\left[\frac{2B_0^2\tilde{\omega}_y^2 + \tilde{\omega}_x^2 - iB_0\tilde{\omega}_x\tilde{\omega}_y}{4B_0^2\tilde{\omega}_y^2 + \tilde{\omega}_x^2}\right] \\ &\quad + \frac{3iB_1C_{30}\tilde{\omega}_y}{2\tilde{\omega}_x^3} - \frac{3iC_{30}C_{12}}{\tilde{\omega}_x^3\tilde{\omega}_y} - \frac{2B_0B_1C_{12}\tilde{\omega}_y}{\tilde{\omega}_x^2}\left[\frac{2B_0\tilde{\omega}_y + i\tilde{\omega}_x}{4B_0^2\tilde{\omega}_y^2 + \tilde{\omega}_x^2}\right].\end{aligned} \tag{21}$$

Finally, writing the terms proportional to R^0 as $\gamma+\gamma' = c + L(L+1)$, we have

$$2R^2\varepsilon'_{\mathrm{asy}}(R) = aR + bR^{1/2} + c + L(L+1), \tag{22}$$

where the L-independent coefficients are $a=-6.660\,38$, $b=9.5552-i7.4593$, and $c=-3.8566+i11.852$. We note that in the expansion of $2R^2\varepsilon'_{\mathrm{asy}}(R)$ to order R^0 the only L dependence is just the simple real term $L(L+1)$. This is the first deviation of the expansion of $2R^2\varepsilon'_{\mathrm{asy}}(R)$ to order R^0 that involves the off-diagonal adiabatic coupling. Retaining only the diagonal term would give $D_0L(L+1)$ in Eq. (22) rather than $L(L+1)$.

B. The HHCM ionization cross section and extended threshold law

The HHCM absolute partial-wave ionization cross section is given by

$$\sigma^L(E) = \frac{(2L+1)}{(1+2E)}\pi P^L(E)\int |\varphi_{\mathrm{asy}}(R_E;\Omega_E)|^2 d\Omega_E, \tag{23}$$

where $P^L(E)$ is the ionization probability. The asymptotic eigenfunction $\varphi_{\mathrm{asy}}(R_E;\Omega_E)$ is evaluated at $R=R_E$, where $R_E=4R_W$ and $R_W=C_{00}/E$ is the Wannier radius. The angular coordinates Ω_E are those associated with the wave vectors $\mathbf{k}_+$ and $\mathbf{k}_-$ of the outgoing positron and electron [5,6]. The element of integration is $d\Omega_E = d\alpha_E d\hat{\mathbf{k}}_+ d\hat{\mathbf{k}}_-$, where $\tan\alpha_E = k_-/k_+$. The part of $\varphi_{\mathrm{asy}}(R_E;\Omega_E)$ that depends on $\hat{\mathbf{k}}_+$ and $\hat{\mathbf{k}}_-$ can be real and the modulus square is normalized to unity with respect to $\hat{\mathbf{k}}_+$ and $\hat{\mathbf{k}}_-$. However, the part of $\varphi_{\mathrm{asy}}(R_E;\Omega_E)$ that depends on α_E is complex and the square is normalized to unity with respect to α_E. Since Eq. (23) involves the modulus square of $\varphi_{\mathrm{asy}}(R_E;\Omega_E)$, the integration of $|\varphi_{\mathrm{asy}}(R_E;\Omega_E)|^2$ over Ω_E is

$$\int |\varphi_{\text{asy}}(R_E;\Omega_E)|^2 d\Omega_E = |N_{n_x=0}|^2 \frac{\pi}{2} = \pi^{1/2}\left(\frac{C_{20}C_{00}}{2E}\right)^{1/4}. \tag{24}$$

(Unlike Ref. [5] for electron-hydrogen ionization, we do not introduce the factor $\sin 2\alpha_E$ in the integrand of Eq. (24) because the positron-hydrogen potential is not symmetric.) The HHCM absolute partial-wave ionization cross section can now be written as

$$\sigma^L(E) = (2L+1)\pi^{3/2}\left(\frac{C_{20}C_{00}}{2E}\right)^{1/4}\frac{P^L(E)}{(1+2E)}. \tag{25}$$

In the HHCM treatment of positron-hydrogen ionization near threshold, we consider that ionization proceeds via the second channel, which is the level associated with ground-state positronium formation. The paths that we are considering for the positron-ionization calculation are similar to those that are important in electron-impact ionization. These paths are dominant for positron-impact ionization. However, there are additional paths that go through a tunneling region (under the barrier transitions) that do not occur for electron-impact ionization. The contribution of these paths is expected to be small and therefore is neglected in the present calculation.

The ionization probability $P^L(E)$ for positron-impact ionization of hydrogen is

$$P^L(E) = P_{Ps}(E)\exp(-2\,\text{Im}[A]), \tag{26}$$

where $P_{Ps}(E)$ is the probability for the intermediate transition from the ground state of hydrogen to the ground state of positronium and A is the action integral given below. Both $P_{Ps}(E)$ and A are L dependent.

Only in the Ore gap is $P_{Ps}(E)$ equivalent to the probability for ground-state positronium formation. For the energy above the ionization threshold, $P_{Ps}(E)$ also includes contributions from all processes that proceed via the ground-state positronium channel.

In the HHCM framework, the transition probability $P_{Ps}(E)$ for intermediate ground-state positronium formation is obtained by summing Wentzer-Kramers-Brillouin (WKB)-like functions of the form $e^{i\int K(R)dR}$ over two different paths that connect level 1 [e^+-H($1s$)] with level 2 [H^+-Ps($1s$)] [19,21], where the L-dependent wave vector $K(R)$ is

$$K^2(R) = 2[E - \varepsilon'(R)]. \tag{27}$$

We compute $\varepsilon'(R)$ by solving $L+1$ coupled partial differential equations of Eq. (7) with the finite element analysis [20,21]. The transition probability for intermediate ground-state positronium formation is given by [19,21]

$$P_{Ps}(E) = 4P_{12}(1-P_{12})\sin^2\Delta_{12}, \tag{28}$$

where P_{12} is the one-way transition probability

$$P_{12} = \exp\left[-\text{Im}\int_C K(R)dR\right] \tag{29}$$

and Δ_{12} is the Stückelberg phase

$$\Delta_{12} = \text{Re}\int_C K(R)dR. \tag{30}$$

Both P_{12} and Δ_{12} are L dependent. The contour C of integration in Eqs. (29) and (30) is from the classical turning point of the sheet of the Riemann surface $\varepsilon'(R)$ corresponding to level 1, around the branch point R_b, to the classical turning point on the sheet corresponding to level 2. The transition probability $P_{Ps}(E)$ varies slowly with energy above the ionization threshold.

The action integral A in Eq. (26) is given by

$$A = \int_{R_0}^{\infty}[K(R) - K_0(R)]dR. \tag{31}$$

The integration of Eq. (31) is along a path in the complex R plane that starts at $R=R_0+i0$, a point slightly to the right of the real part of the branch point R_b that connects level 1 to level 2, and goes out to infinity through the harmonic oscillator region (which is where Im[R] is large). We show the beginning of this path in Fig. 2(a) which gives the Riemann plot of Re[$\varepsilon'(R)$] for levels 1 and 2. Figure 2(b) compares Re[$\varepsilon'(R)$] for level 2 with Re[$\varepsilon'_{\text{asy}}(R)$] given by Eq. (22). For sufficiently large Im(R), $\varepsilon'_{\text{asy}}(R)$ is a good approximation to $\varepsilon'(R)$. The region where this approximation holds is called the harmonic oscillator region. $\varepsilon'_{\text{asy}}(R)$ does not contain any branch points.

The wave vector $K(R)$ of Eq. (31) is defined according to Eq. (27), where the eigenvalue $\varepsilon'(R)$ is associated with level 2. The zeroth-order wave vector $K_0(R)$ is defined by

$$K_0^2(R) = 2[E - \varepsilon'_0(R)], \tag{32}$$

where

$$\varepsilon'_0(R) = -\frac{C_{00}}{R} = \frac{a}{2R}. \tag{33}$$

At R_{asy}, where Re[R_{asy}]=R_0 and Im[R_{asy}] is sufficiently large so that R_{asy} is in the harmonic oscillator region, the exact eigenvalue $\varepsilon'(R)$ can be replaced by its asymptotic value $\varepsilon'_{\text{asy}}(R)$ given in Eq. (22). Replacing $\varepsilon'(R)$ by $\varepsilon'_{\text{asy}}(R)$, Eq. (31) can be written in the form

$$A = \int_{R_0}^{R_{\text{asy}}}[K(R) - K_0(R)]dR + \int_{R_{\text{asy}}}^{\infty}[K_{\text{asy}}(R) - K_0(R)]dR, \tag{34}$$

where $K_{\text{asy}}(R)$ is defined according to

$$K^2_{\text{asy}}(R) = 2[E - \varepsilon'_{\text{asy}}(R)]. \tag{35}$$

Since the asymptotic eigenvalue $\varepsilon'_{\text{asy}}(R)$ has no branch points, we can choose any path from R_{asy} to $R=\infty+i0$ for the second integral of Eq. (34). We choose specifically a path from R_{asy} back to R_0, then along the real axis to some very large real R_c, and then finally out to infinity. We show this path in Fig. 3. The action integral A for this path can be written in the form

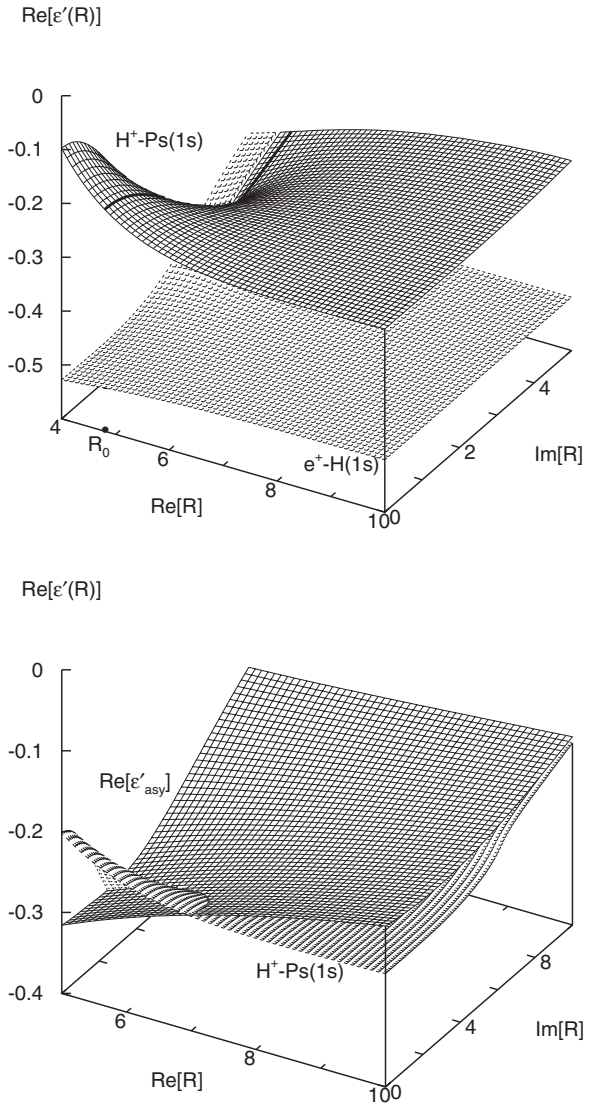

FIG. 2. (a) For $L=0$, Riemann plot of $\mathrm{Re}[\varepsilon'(R)]$ vs complex R, for level 1 [e^+-H($1s$)] and level 2 [H^+-Ps($1s$)]. The integration path shown starts at $R=R_0+i0$ and goes along the line $R=R_0+i\,\mathrm{Im}\,R$. (b) For $L=0$, $\mathrm{Re}[\varepsilon'(R)]$ for level 2 and $\mathrm{Re}[\varepsilon'_{\mathrm{asy}}(R)]$ vs complex R.

$$A = \int_{R_0}^{R_{asy}} [K(R) - K_0(R)]dR + \int_{R_{asy}}^{R_0} [K_{asy}(R) - K_0(R)]dR + \int_{R_0}^{R_c} [K_{asy}(R) - K_0(R)]dR + \int_{R_c}^{\infty} [K_{asy}(R) - K_0(R)]dR$$
$$= \int_{R_0}^{R_{\mathrm{asy}}} [K(R) - K_{\mathrm{asy}}(R)]dR + \int_{R_0}^{R_c} [K_{\mathrm{asy}}(R) - K_0(R)]dR + \int_{R_c}^{\infty} [K_{\mathrm{asy}}(R) - K_0(R)]dR. \quad (36)$$

For the third integral, where the range of R is from R_c to infinity, $K_{\mathrm{asy}}(R)$ can be replaced by its Taylor's expansion $K_c(R)$,

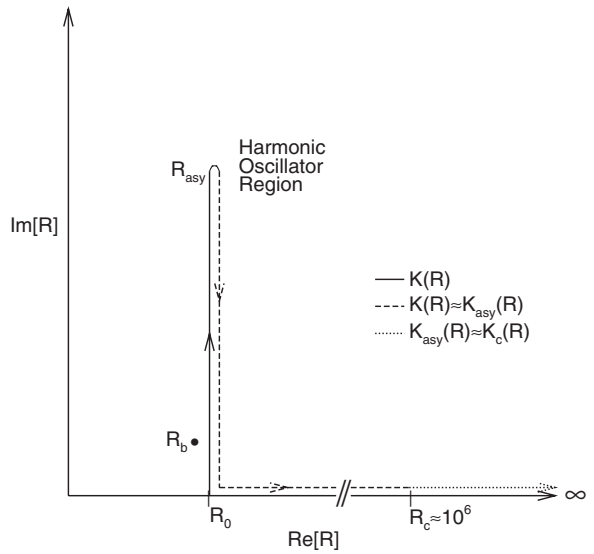

FIG. 3. Integration path in the complex R plane for the action integral A; see discussion before Eq. (36).

$$K_c(R) = K_0(R) - \frac{1}{K_0(R)}\left(\frac{b}{2R^{3/2}} + \frac{c}{2R^2}\right) - \frac{1}{2K_0^3(R)}\left(\frac{b}{2R^{3/2}}\right)^2. \quad (37)$$

The importance of replacing $K_{\mathrm{asy}}(R)$ by $K_c(R)$ in the third integral is that one can evaluate the integral analytically. Before we extract the Wannier and extended Wannier threshold laws, we add and subtract the term $\int_{R_0}^{R_c}[K_c(R)-K_0(R)]dR$ to Eq. (36), and recast the action integral in the form

$$A = A_1 + A_2 + A_3 = \int_{R_0}^{R_{\mathrm{asy}}} [K(R) - K_{\mathrm{asy}}(R)]dR + \int_{R_0}^{R_c} [K_{\mathrm{asy}}(R) - K_c(R)]dR + \int_{R_0}^{\infty} [K_c(R) - K_0(R)]dR. \quad (38)$$

The first two integrals A_1 and A_2 vary slowly with energy and the energy dependence of the action integral comes primarily from A_3.

Using Eqs. (26) and (38), we can write the ionization probability $P^L(E)$ as

$$P^L(E) = P^L_{\mathrm{inner}}(E) P_{\mathrm{asy}}(E), \quad (39)$$

where

$$P^L_{\mathrm{inner}}(E) = P_{Ps}(E)\exp[-2\,\mathrm{Im}(A_1 + A_2)], \quad (40)$$

and

$$P_{\mathrm{asy}}(E) = \exp[-2\,\mathrm{Im}\,A_3] = \exp\left[-2\,\mathrm{Im}\int_{R_0}^{\infty}[K_c(R) - K_0(R)]dR\right]. \quad (41)$$

Substituting Eq. (39) into Eq. (25), we can write the HHCM absolute partial-wave ionization cross section in the form

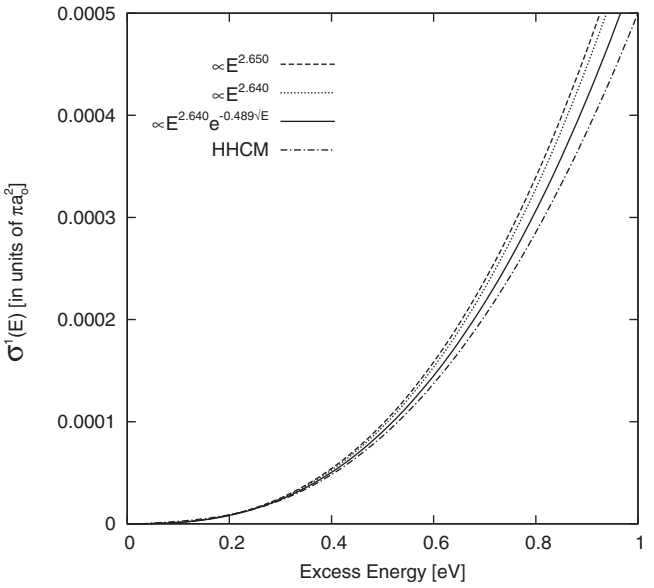

FIG. 4. The HHCM absolute P-wave cross section $\sigma^1(E)$ of Eq. (42) compared with the Wannier and extended Wannier threshold laws. (The threshold laws are normalized to $\sigma^1(E)$ at $E=0.0272$ eV.)

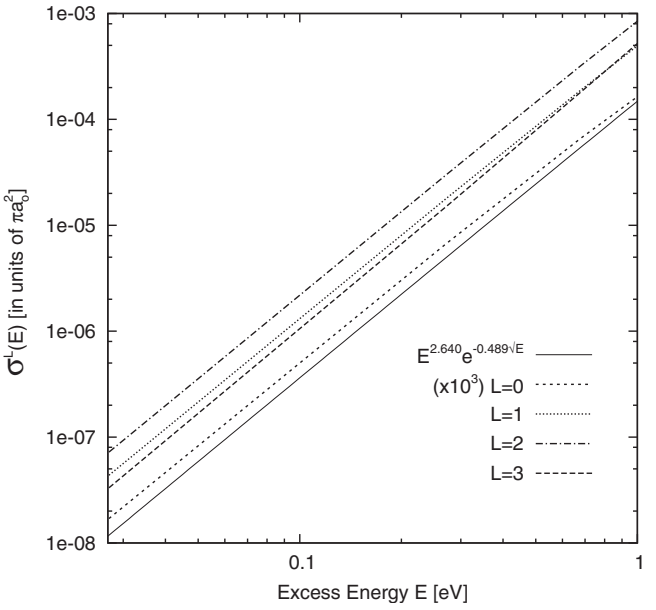

FIG. 5. The HHCM absolute partial-wave cross sections $\sigma^L(E)$ of Eq. (42) compared to the extended Wannier threshold law of Eq. (43). (The Wannier and extended Wannier threshold laws are indistinguishable on the log-log plot.)

$$\sigma^L(E) = (2L+1)\pi^{3/2}\left(\frac{C_{20}C_{00}}{2E}\right)^{1/4} \frac{P^L_{\text{inner}}(E)P_{\text{asy}}(E)}{(1+2E)}. \tag{42}$$

$P^L_{\text{inner}}(E)$ is a slowly varying function of energy, which allows us to treat $P^L_{\text{inner}}(E)/(1+2E)$ as a constant near threshold. If in addition, we retain only the lowest order E dependent terms in $P_{\text{asy}}(E)$, we obtain the L-independent extended Wannier threshold law

$$\sigma(E) \propto E^{2.640}\exp[-0.489\sqrt{E}]. \tag{43}$$

This is the first rigorous proof that the extended Wannier threshold law is independent of L. This threshold law was obtained by Ihra *et al.* [6] for the special case $L=0$. The coefficient of the exponential in Ref. [6] was incorrect; the correct value of −0.489 is given in Ref. [15] for $L=0$. The threshold exponent $\zeta=2.640$ differs by less than 0.4% from the Wannier exponent for positrons $\zeta=2.650\,11$. This is remarkable agreement given that for electron-hydrogen ionization, the threshold exponent obtained from the HHCM differs by about 2% from the Wannier exponent.

III. RESULTS

We calculate the HHCM absolute ionization cross section given in Eq. (42). In these calculations, we evaluate $P^L_{inner}(E)$ and $P_{asy}(E)$ using Eqs. (40) and (41), respectively. We obtain the wave vector for $K(R)$ that appears in A_1 of Eq. (40) by solving the $L+1$ coupled partial differential equations given in Eq. (7).

In Fig. 4, we compare the P-wave HHCM absolute ionization cross section of Eq. (42) with both the Wannier threshold law of Eq. (1) and the extended Wannier threshold law of Eq. (43). We normalize the two threshold laws to the absolute HHCM P-wave cross section at $E=0.001$ a.u. (While we perform the calculation in atomic units, we plot the cross sections in units of πa_0^2 and excess energy in units of eV.) The HHCM P-wave ionization cross section is in accord with both threshold laws. The extended Wannier threshold law is a slight improvement over the Wannier threshold law. This is not only the case for $L=1$, but also for the other partial waves ($L=0$, 2, and 3). For the energy range $0 \leqslant E \leqslant 1$ eV, the Wannier and extended Wannier threshold laws are indistinguishable on a log-log plot.

In Fig. 5, we compare the HHCM absolute partial-wave ionization cross sections of Eq. (42) for $0 \leqslant L \leqslant 3$ with the extended Wannier threshold law of Eq. (43). The HHCM gives the correct threshold behavior for all L. Furthermore, the partial-wave ionization cross sections can be obtained at energies arbitrarily close to zero. We note that the S-wave contribution is extremely small; the dominant contribution comes from the D wave.

The small S-wave contribution was also observed in two S-wave model CCC calculations (see Fig. 6); the first calculation retained only hydrogen and positronium s states [13]; the second included s, p, and d states [14]. While the HHCM S-wave ionization cross section is significantly smaller than the CCC results, the contribution of the S wave to the total ionization cross section is negligible. The HHCM provides an important insight into the very small ionization cross section. Recall that the transition probability for intermediate ground-state positronium formation $P_{Ps}(E)$ is directly proportional to $\sin^2\Delta_{12}$. The Stückelberg phase Δ_{12} for $L=0$ is close to π [19] (see Fig. 7). This means that the WKB-like functions for the two paths that connect level 1 [e^+-H($1s$)] with level 2 [H^+-Ps($1s$)] interfere destructively [19,21]. Thus any process, including ionization, that proceeds via the

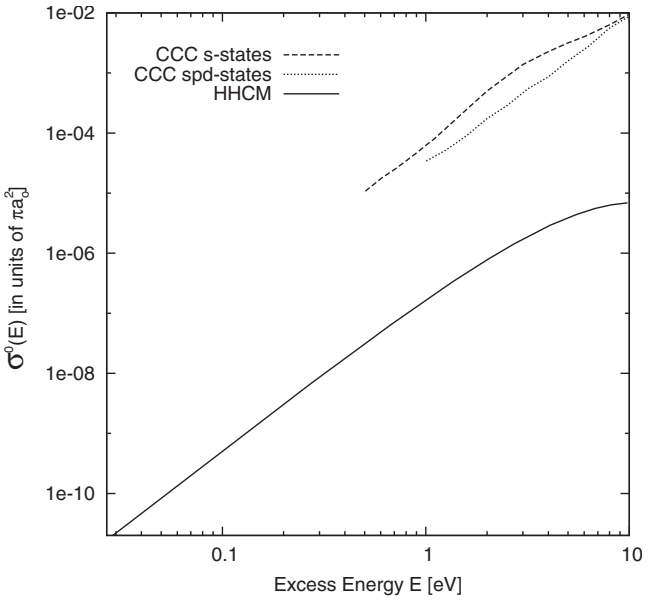

FIG. 6. The HHCM absolute S-wave cross section $\sigma^0(E)$ of Eq. (42) compared with the S-wave model CCC(H+Ps) calculations. In one S-wave model CCC calculation, the s states of H and Ps are retained; in the other S-wave model CCC calculation, the s, p, and d states are retained.

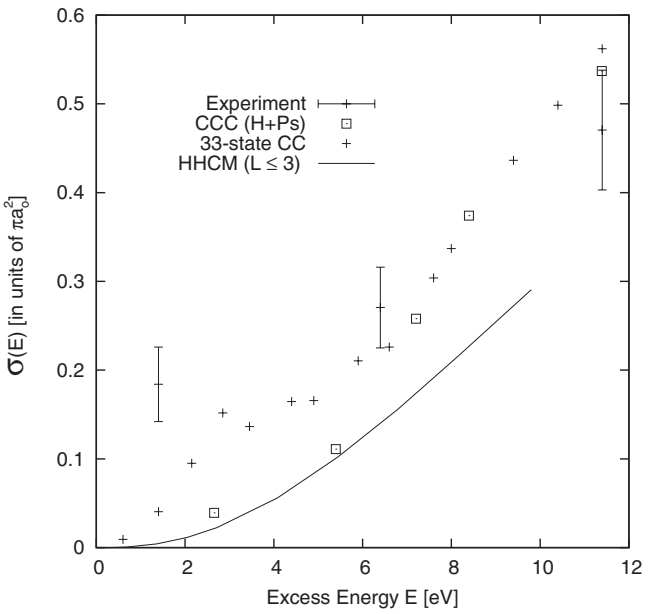

FIG. 8. The HHCM absolute ionization cross section $\sigma(E)$ summed over $0 \leqslant L \leqslant 3$ compared with the total ionization cross section of the CCC(H+Ps) and the 33-state CC calculations and experimental data.

ground-state positronium channel is very small. We also note that the magnitude of the cross section is *extremely* sensitive to small variations in the Stückelberg phase when Δ_{12} is very close to integer multiples of π. This could account for the difference between the HHCM and the CCC results.

We can also explain the large D-wave contribution in terms of the Stückelberg phase. As we show in Fig. 7, for $L=2$, Δ_{12} is close to $\pi/2$ [19]. The WKB-like functions for the two paths that connect levels 1 and 2 interfere constructively and the probability for any process that proceeds through the ground-state positronium channel is near maximum. The dependence of the Stückelberg phase on L indicates that the contribution from the next few partial waves $L>3$ should be smaller than the P, D, or F waves.

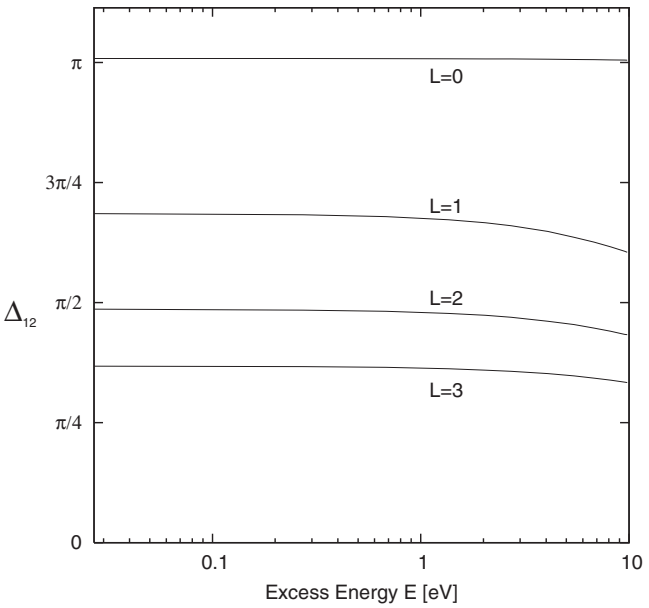

FIG. 7. Stückelberg phase Δ_{12} given by Eq. (30) for intermediate ground-state positronium formation and ionization.

In Fig. 8, we show the HHCM ionization cross section summed over the partial waves $L=0$, 1, 2, and 3 and compare it with the total ionization cross section obtained by the CCC [12,13] and the 33-state CC calculations [11], both of which are converged with respect to L. We also show in Fig. 8 the experimental measurements of the total ionization cross section [3]. The HHCM ionization cross section is a smooth function of energy, even close to threshold. In the limit $E \rightarrow 0$, the HHCM obeys the Wannier threshold law. The HHCM and CCC are in reasonable agreement at low energies; the 33-state CC calculation appears to have some spurious structure near 3 eV and does not satisfy the Wannier threshold law. At the higher energies, the 33-state CC and CCC calculations are in good agreement with experimental measurements. As expected, the HHCM is lower because the calculation includes only partial waves up to $L=3$; the HHCM cross section is not converged with respect to L. Higher partial waves are particularly important for positron-hydrogen ionization because the S-wave cross section is extremely small.

IV. CONCLUSIONS

Using the HHCM, we have calculated the absolute partial-wave cross section for positron-hydrogen ionization near threshold for $L=0$, 1, 2, and 3. Furthermore, we have also shown analytically that the extended Wannier threshold law is L independent.

The HHCM partial-wave ionization cross sections satisfy the Wannier threshold and extended Wannier threshold laws,

and can be computed at energies arbitrarily close to zero energy. The calculation confirms that the HHCM can be successfully applied at energies extremely close to threshold, which is a very important feature of the method.

The HHCM ionization cross section summed over the partial waves $L=0,1,2$, and 3 is in good agreement with the CCC total ionization cross section [12,13] at low energies. At higher energies, the HHCM ionization cross section is in reasonable agreement with the CCC [12,13] and the 33-state CC [11] total ionization cross section and experimental measurements [3]. As expected, the HHCM results (which include only the first four partial waves) lie below the calculations which are fully converged with respect to L. The contribution of the higher partial waves increases with increasing energy.

The HHCM calculations provide an interpretation of the very small S-wave contribution to the ionization cross section and the dominant D-wave contribution in terms of destructive and constructive interference, respectively.

We conclude that the HHCM describes with success near-threshold positron-hydrogen ionization and provides important insight into the ionization process.

ACKNOWLEDGMENTS

We appreciate discussions with Dr. S. Yu. Ovchinnikov and we are thankful to Dr. A. S. Kadyrov, Dr. G. Laricchia, and Dr. H. R. J. Walters for providing us with tables of their published data. S.J.W. and J.S. acknowledge support from the National Science Foundation, under a collaborative grant (Grants No. PHYS-0440565 and No. PHYS-0440714). J.H.M. acknowledges support from the Chemical Science, Geosciences and Biosciences Division, Office of Basic Energy Sciences, Office of Science, U.S. Department of Energy under Grant No. DE-FG02-02ER15283. Oak Ridge National Laboratory is managed by UT Battle LCC under Contract No. DE-AC05-00OR22725. S.J.W. acknowledges the use of the UNT academic computing facilities.

[1] G. H. Wannier, Phys. Rev. **90**, 817 (1953).
[2] H. Klar, J. Phys. B **14**, 4165 (1981).
[3] G. O. Jones, M. Charlton, J. Slevin, G. Laricchia, À. Kövér, M. R. Poulsen, and S. Nic Chormaic, J. Phys. B **26**, L483 (1993).
[4] J. M. Rost and E. J. Heller, Phys. Rev. A **49**, R4289 (1994).
[5] J. H. Macek and S. Yu. Ovchinnikov, Phys. Rev. A **54**, 544 (1996).
[6] W. Ihra, J. H. Macek, F. Mota-Furtado, and P. F. O'Mahony, Phys. Rev. Lett. **78**, 4027 (1997).
[7] P. Ashley, J. Moxom, and G. Laricchia, Phys. Rev. Lett. **77**, 1250 (1996).
[8] N. C. Deb and D. S. F. Crothers, J. Phys. B **35**, L85 (2002).
[9] Jim Mitroy, J. Phys. B **29**, L263 (1996).
[10] Ann A. Kernoghan, Mary T. McAlinden, and H. R. J. Walters, J. Phys. B **28**, 1079 (1995).
[11] Ann A. Kernoghan, D. J. R. Robinson, Mary T. McAlinden, and H. R. J. Walters, J. Phys. B **29**, 2089 (1996).
[12] A. S. Kadyrov and I. Bray, Phys. Rev. A **66**, 012710 (2002).
[13] A. S. Kadyrov, I. Bray, and A. T. Stelbovics, Phys. Rev. Lett. **98**, 263202 (2007).
[14] A. S. Kadyrov, I. Bray, and A. T. Stelbovics, J. Phys.: Conf. Ser. **88**, 012062 (2007).
[15] James Sternberg, S. J. Ward, J. H. Macek, and J. Shertzer, Bull. Am. Phys. Soc. **49**, 52 (2004).
[16] S. J. Ward, Krista Jansen, J. Shertzer, and J. H. Macek, Nucl. Instrum. Methods Phys. Res. B **266**, 410 (2008).
[17] J. H. Macek, S. Yu. Ovchinnikov, and S. V. Pasovets, Phys. Rev. Lett. **74**, 4631 (1995).
[18] J. H. Macek, Few-Body Syst. **31**, 241 (2002).
[19] S. J. Ward, J. H. Macek, and S. Yu. Ovchinnikov, Phys. Rev. A **59**, 4418 (1999).
[20] S. J. Ward and J. Shertzer, Phys. Rev. A **68**, 032720 (2003).
[21] S. J. Ward, J. Shertzer, S. Yu. Ovchinnikov, and J. H. Macek, Phys. Rev. A **75**, 012713 (2007).
[22] U. Fano, D. Green, J. L. Bohn, and T. A. Heim, J. Phys. B **32**, R1 (1999).
[23] Yan Zhou and C. D. Lin, J. Phys. B **27**, 5065 (1994).
[24] A. K. Bhatia and A. Temkin, Rev. Mod. Phys. **36**, 1050 (1964).
[25] George B. Arfken and Hans J. Weber, *Mathematical Methods for Physicists*, 6th Ed. (Elsevier Academic, Boston, 2005), p. 841.